Source inversion of intensity patterns of earthquakes: A destructive shock in 1936 in northeast Italy

Livio Sirovich and Franco Pettenati

Istituto Nazionale di Oceanografia e di Geofisica Sperimentale, Trieste, Italy

Received 1 December 2003; revised 26 May 2004; accepted 28 June 2004; published 21 October 2004.

[1] We demonstrate that it is possible to retrieve geometric and kinematic information about the source of a destructive past earthquake by inverting its regional macroseismic intensity patterns. In fact, in the case study the inversion results agree with the seismological instrumental measurements of the 1930s and with neotectonic evidence. This leads to the hope that more knowledge about preinstrumental events can be obtained: a key toward improving the calculation of seismic hazard, mostly in the Old World. After validating our technique on the 1987 Whittier Narrows, California, earthquake [*Pettenati and Sirovich*, 2003; *Gentile et al.*, 2004] we achieve the present results by investigating an earthquake that happened in 1936 in northeast Italy. The automatic inversions were performed by using a simplified formula for body waves that radiate from a linear source. The inversion shows two minima on the hypersurface of the minimum residuals (calculated – observed intensity at all sites) in the multiparameter model space. These two minimum variance source models resemble the two auxiliary planes of the same theoretical fault plane solution, similar to that given by the standard use of the first *P* wave arrivals. The present result encourages us to treat more cases and to explore new inversion techniques for quantitatively treating the intensity patterns of earthquakes because, at least in some cases, they carry geometric and kinematic information about their source. *INDEX TERMS:* 7230 Seismology: Seismicity and seismotectonics; 7260 Seismology: Theory and modeling; 8123 Tectonophysics: Dynamics, seismotectonics; 3260 Mathematical Geophysics: Inverse theory; *KEYWORDS:* Alps, 1936, macroseismic intensity, source inversion, Aviano Overthrust

Citation: Sirovich, L., and F. Pettenati (2004), Source inversion of intensity patterns of earthquakes: A destructive shock in 1936 in northeast Italy, *J. Geophys. Res.*, *109*, B10309, doi:10.1029/2003JB002919.

1. Introduction

[2] This paper is a step toward developing the quantitative treatment of the so-called macroseismic intensity, *I*, to retrieve geophysical information about the source of mostly preinstrumental earthquakes [*Pettenati et al.*, 1999; *Sirovich and Pettenati*, 2001]. We have already validated the automatic source inversions of the regional intensity pattern of the 1987 Whittier Narrows, California, earthquake [*Pettenati and Sirovich*, 2003; *Gentile et al.*, 2004]. Here we test our technique for the second time by inverting the intensities of the 18 October, 0310:53.6 UT 1936 event in the Cansiglio Plateau area in northeast Italy. The data come from *Barbano et al.* [1986] and are now available on the Web in the DOM4.1 catalog (G. Monachesi and M. Stucchi, unpublished data, 1997) (see http://emidius.mi.ingv.it/DOM/home.html). A magnitude range between M_s = 5.8, and M_m = 6.2 for the 1936 earthquake is reported by the NT4.1 catalog (R. Camassi and M. Stucchi, unpublished data, 1997) (see http://emidius.mi.ingv.it/NT/home.html). M_s is surface wave magnitude; M_m is "macroseismic magnitude" obtained from an empirical correlation between M_s values and epicentral intensities, with a standard deviation of 0.39 (R. Camassi and M. Stucchi, unpublished data, 1997). A wider magnitude range is found in the literature (see Table 3).

[3] The studied earthquake is a key event for the seismotectonics and the seismic hazard of the area; in fact, it is one of the two strong 20th century events preceding the one which caused 1000 casualties in Friuli in 1976. See the epicenters of the 1928 (M_s = 5.6), 1936 (M_s = 5.8), and 1976 (M_s = 6.5) earthquakes in the inset of Figure 1, where the patterned area shows the outcropping Alps and External Dinarides. The coordinates and surface wave magnitudes are taken from the most recent Italian parametric catalog by *Boschi et al.* [1999].

[4] Generally, the starting point for our work, from the point of view of inversions, was the consideration that in several cases the traditional isoseismals of some well-surveyed earthquakes bore a likeness to synthetic isoseismals (see some examples of this by *Ohta and Satoh* [1980], *Chiaruttini and Siro* [1991], and *Panza et al.* [1991]). In particular, they bore a likeness to those obtained from our kinematic function *KF*, which calculates the shear body waves radiated by an extended linear source [*Sirovich*, 1996a, 1996b, 1997].

[5] Since the inversion problem is nonlinear, we looked for the minimum residuals (calculated minus observed

0148-0227/04/2003JB002919$09.00

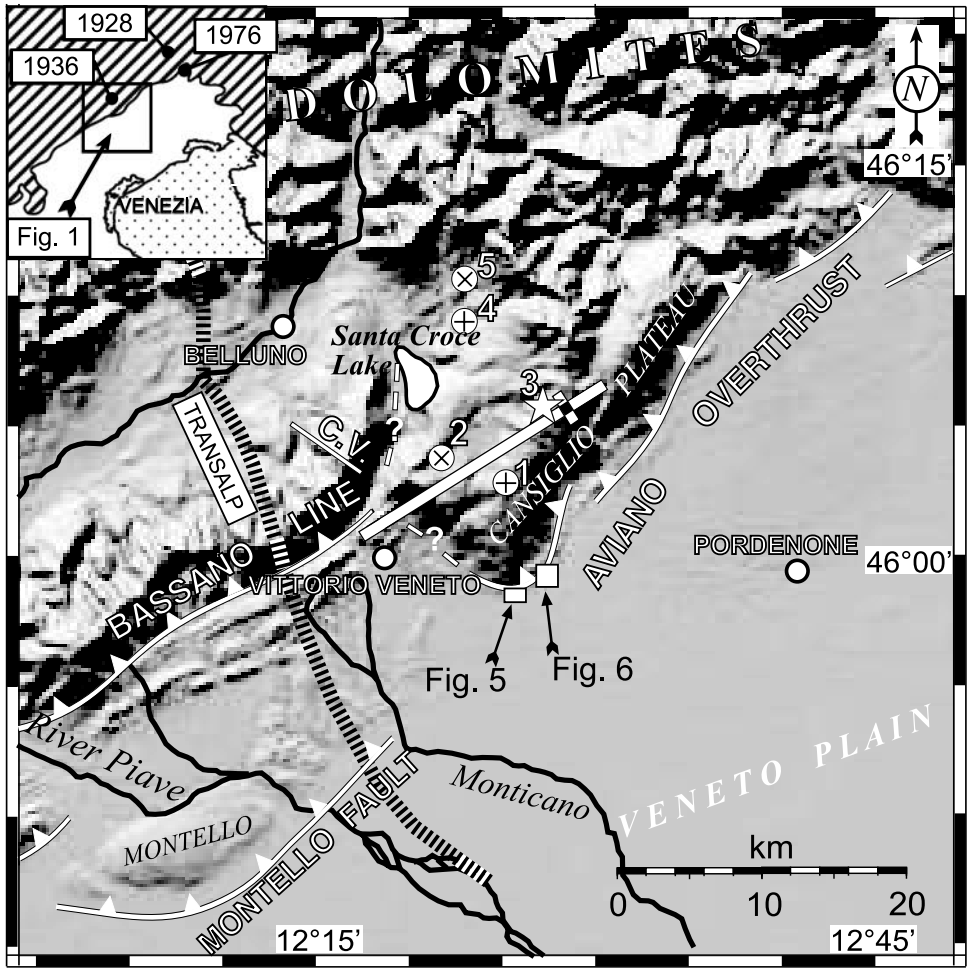

Figure 1. Tectonic sketch of the studied area; see the segmented Aviano Overthrust. Macroseismic epicenters are as follows: (1) Bosco Cansiglio, 1936 earthquake from the CFTI catalog; (2) the same as (1), but from the NT4.1 catalog; (4) Belluno, 1873 earthquake from CFTI; (5) the same as (4), but from the NT4.1 catalog. The white star (3) is the instrumental epicenter. See the positions of Figures 5 and 6. For the river diversion and for the fault "C.V.," see details and references in the text.

intensity at all sites) in the 11-source parameter model space by employing a sharing niching genetic algorithm (NGA) (see section 2.2). Consider that we call "pseudo-intensity" the macroseismic intensity treated as a real or integer number.

[6] Figure 1 shows the epicenters of the earthquake in question according to the CFTI catalog by *Boschi et al.* [1995] (see number 1 in the figure) and the NT4.1 (R. Camassi and M. Stucchi, unpublished data, 1997) (number 2). Both came from regional intensity patterns. The instrumental epicenter (number 3), on the other hand, is from *Slejko et al.* [1989] (confirmed by *Renner* [2000]). Figure 1 also shows the southern part of the path of the TRANSALP European 340-km-long crustal seismic profile [*TRANSALP Working Group*, 2001]. The figure also shows the so-called Bassano Line and a recent hypothesis on the segmentation of the so-called Aviano Overthrust, which approximately marks the piedmont line of the Veneto Plain. The insets in Figure 1 show some neotectonic symptoms (see Figures 5 and 6). The thick segment in white is the projection of the line source, which was found by inversion, on the Earth's surface; the small black square, along the white segment, is the projection of the nucleation point; note the prevalent propagation of the rupture toward the southwest (see section 6.2).

[7] In the following we show that our automatic inversion of intensity data can roughly identify the parameters of the causative source of the studied earthquake with a quality comparable to that obtained by treating early instrumental measurements with basic seismological techniques. We retrieve the following source parameters with no constraints: the hypocentral latitude and longitude and the fault plane solution (strike, dip, and rake angle). Then, we retrieve more source parameters within reasonable constraints: the seismic moment, M_0, the depth of the line source, H, the shear wave velocity, V_S, the rupture velocities V_r, and rupture lengths along-strike and antistrike. Finally, the studied earthquake offers the opportunity to compare the source obtained from the inversion of intensity with (1) that deducible from instrumental observations of 1936, (2) seismotectonic interpretations independent from this study, and (3) some neotectonic indicators.

[8] In a different study [*Pettenati and Sirovich*, 2003; *Gentile et al.*, 2004] we demonstrated that the introduction of asymmetric rupture lengths and propagations in our

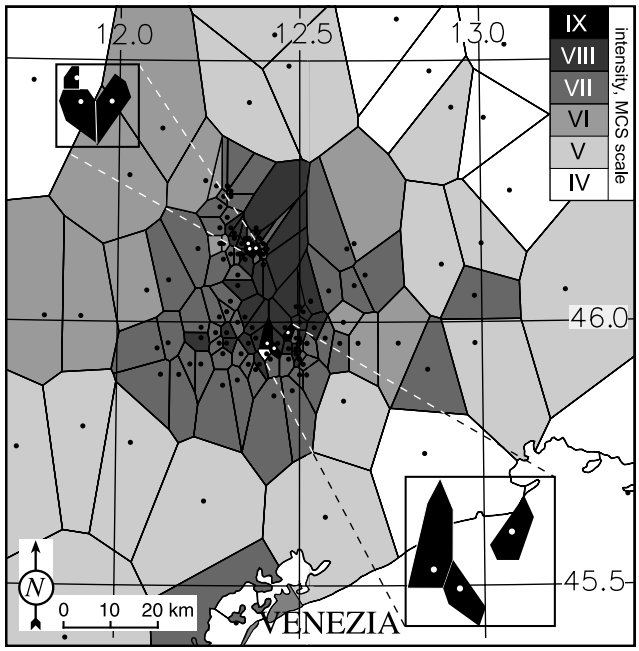

Figure 2. Bosco Cansiglio M_s = 5.8 1936 earthquake. Tessellated observed intensities are from the DOM4.1 catalog (G. Monachesi and M. Stucchi, unpublished data, 1997).

model did not substantially change the typical bimodal nature of the inversion of the fault plane solution, already investigated by *Koper et al.* [1999]. In particular, we first understood that in our model the ambiguity of the solution decreases the more the rake angle differs from the 90° (±180°) value and, second, the more the rupture is asymmetric (see section 7.1).

[9] In this paper we do automatic inversions and for this, given the bimodal nature of the problem, we implemented a code based on a sharing NGA, with separate subpopulations of sources; in particular, we used some routines from the Parallel Genetic Algorithm Library by *Levine* [1996].

2. The *KF* Function and the Inversion Procedure

2.1. The *KF* Function

[10] Since the *KF* formula and its use in the source inversion of regional intensity patterns have already been presented in different journals, we refer the reader to *Sirovich* [1996a, 1996b, 1997] for *KF* and to *Pettenati et al.* [1999], *Sirovich and Pettenati* [2001], *Pettenati and Sirovich* [2003], and *Gentile et al.* [2004] for the inversion technique. With respect to the *KF* formula, we only want to stress here that it agrees with the asymptotic approximation [*Madariaga and Bernard*, 1985; *Spudich and Frazer*, 1984] by assuming that the seismic source is a dislocation propagating horizontally on a rupture plane of unit width. We also recall that in our convention (1) the fault plane is dipping to the right of the positive direction of the strike, which ranges between 0° and 360° and (2) the rake angle is seen on the fault plane from the hanging wall of the fault and measured anticlockwise from 0° to 360° between the positive direction of the strike and the direction of the slip vector $\bar{\mathbf{u}}$. In this approach, only the body wave radiation from a line source in an elastic half-space in the distance range of ~5–100 km and wavelengths shorter than the shortest observer-source distance are considered. For this reason, in the present study, we omitted the sites of the DOM4.1 data bank, which are beyond the borders of Figure 2; thus we used only 140 I data of the DOM4.1 catalog. Then, during inversion, all sites closer than 5 km to the projection of each tentative line source received the maximum *KF* value calculated at the site closest to the source but outside the 5 km limit. Finally, in our convention the total length of the rupture is the sum of the along-strike part, length L_1, and the antistrike length L_2. We also calculate the Mach number$_1$ along-strike and the Mach number$_2$ antistrike (where the Mach number = V_r/V_S). We calculated the pseudo-intensities at location (x, y) from $KF(x, y)$ (referred to a Cartesian plane) with the data-fitting function (2) by *Sirovich et al.* [2001].

[11] It should also be remembered that our *KF* procedure cannot discriminate between the results produced by mechanisms which differ by 180° in the rake angle because in both cases it produces the same radiation but with reversed polarities. This ambiguity may be solved only with additional tectonic/geodynamic information. See the ambiguity of almost pure dip-slip mechanisms later.

[12] Our inversion fitness criterion is the sum of the squared residuals $\sum \mathbf{r}_s^2$, where $\mathbf{r}_s$ is the pseudo-intensity calculated at each site minus the intensity I observed at the same site; the suffix denotes the site. Firstly, we treated the data set directly. In this approach we looked for the source models that minimized the sum of the squared residuals of intensities $\sum \mathbf{r}_s^2$. In the second approach, each squared residual $\mathbf{r}_s^2$ was weighted by the reliability of the macroseismic information at the individual site, given by the authors of the macroseismic study [*Barbano et al.*, 1986] (see section 3.2 and Table 4).

[13] The search for the minima on the hypersurface of the multiparameter model space was free, with some reasonable constraints excepted (see Table 1). We show one example of the structure of the residuals in the multiparameter model space; see Figure 3, which is an example of the final exploration of the whole space of the source parameters of the studied earthquake around the best-fitting model 1 of Table 2. In the figure, model 1 (the hypothesized rupture plane) is marked by the white cross in the three-dimensional parameter model space of the fault plane solution; the arms of the cross represent the error bars. Note that in Figure 3 we show the whole ranges of the strike and rake angles, with a 1° step, and the 37°–52° range for the dip angle, with a 5° step; the last limitation is for graphical purposes, although the whole excursion of the dip angle was

Table 1. Parameter Resolution

Parameter	Incremental Variation
Strike angle, deg	1
Dip angle, deg	1
Rake angle, deg ± 180°	1
Nucleation longitude, deg	0.01
Nucleation latitude, deg	0.01
Nucleation depth H, km	0.1
Rupture length L, km	0.1
V_S, km s^{-1}	0.01
Mach number	0.01
M_0 10^{25} dyne cm	0.01

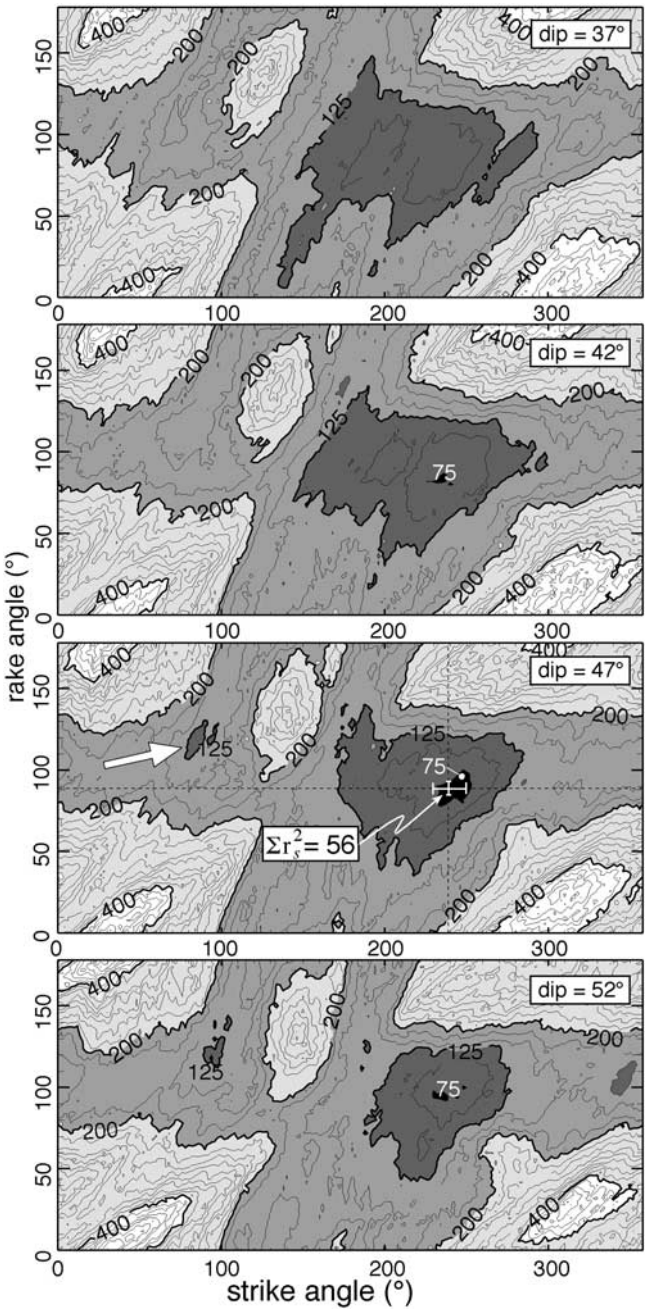

Figure 3. Example of exploration of the whole space of the parameters of the fault plane solution of the studied earthquake and sum of the squared pseudo-intensity residuals $\sum \mathbf{r}_s^2$ at the surveyed sites.

explored with a 1° step. In the case shown the values of $\sum \mathbf{r}_s^2$ go from $\leq$75 (see the small, black depressions) to $\geq$400 (white areas), increasing with steps of 25. Subpopulation 1 finally found its niche in the black depression, scoring $\sum \mathbf{r}_s^2 = 56$ (see Table 2). Figure 3 also hints at the subspace where the NGA subpopulation 2 of Table 2 (with the final strike angle = 62°, dip = 42°, rake = 92°) is also on its way to finding its niche; we refer to the minor depression with $\sum \mathbf{r}_s^2 \leq 125$, which is indicated by the white arrow in the same figure. The jagged paths of the contour lines in Figure 3 are a consequence of the sparse positions of the surveyed sites.

[14] The structure of $\sum \mathbf{r}_s^2$ in the space of the epicentral coordinates resembles Figures 7 and 11 of *Pettenati and Sirovich* [2003] and allows one to find the epicenter in a unique way (figure not shown here for brevity). It turns out to be very close to the instrumental epicenter by *Slejko et al.* [1989], coinciding with that by *Renner* [2000] (see star number 3 in Figure 1).

[15] In this paper we applied the classical bootstrap approach (see section 6.1) to compute the errors of the parameters obtained from our inversions. These are shown in Figure 3.

[16] The total length of the linear source is correlated to M_0. With this in mind, and with the purpose of reducing the total number of parameters to be searched from 12 to 11, we refer to M_0 directly and to the total length obtained with the *Wells and Coppersmith* [1994, p. 990] relationship number 4 (“slip type” = “all”), via the empirical relation $M = 2/3(\log M_0) - 10.7$ by *Hanks and Kanamori* [1979], where M is the moment magnitude. Thus the 11th inversion parameter is the fraction of the along-strike length of the total rupture (the fraction of the antistrike length is the remaining part of the total rupture length).

2.2. Genetic Algorithm Used Here

[17] As known, genetic algorithms (GA) are a randomized search scheme for global nonlinear optimization (see the basic text by *Goldberg* [1989]) and have already been applied to several seismological problems [e.g., *Kennett and Sambridge*, 1992; *Sambridge and Gallagher*, 1993; *Zhou et al.*, 1995; *Bhattacharyya et al.*, 1999; *Koper et al.*, 1999; *Moya et al.*, 2000]. Each source is characterized by a string of 11 unknown source parameters. In brief, three stochastic processes are the evolutionary steps of GA: crossover, mutation, and crowding [see *Gentile et al.*, 2004, Figure 3]. In particular, in keeping with the evolutionary logic, we chose to have the best source of each generation always transmitted to the new generation. The incremental variations shown in Table 1, which correspond to the desired resolutions, were used to vary each source parameter.

[18] In the light of the possible bimodal nature of our problem, we adopted a NGA from the Parallel Genetic Algorithm Library by *Levine* [1996] because the NGA can find more minima. In fact, niching allows different subpopulations of sources to survive within parameter subspaces (niches) so that each source of each subpopulation is not in competition with the sources of other subpopulations living in other niches. We used four subpopulations; each one evolves independently from the others because, in the Sharing step, the normalized distance, D, between each source of a subpopulation and each source of all the other subpopulations obeys the following condition:

$$D(x,y) = \frac{1}{n}\sum_{i=1}^{n}\frac{[x_i - y_i]}{b_i - a_i}, \qquad (1)$$

where n is the number of unknown source parameters (11, in our case), x_i is the ith parameter of a source of subpopulation x, y_i is the ith parameter of a source of subpopulation y; b_i is the upper bound of the ith source parameter, and a_i is the lower bound of the ith parameter [*Koper et al.*, 1999, equation (1)].

[19] D has to be tuned for each study case by trial and error because if the distance D is too high, some subpopu-

Table 2. Source Parameters Corresponding to the Two Absolute Variance Minima in the Niching Genetic Algorithm (NGA) Inversion of the Unweighted Site Intensities

Parameter	Model 1 (Rupture Plane?)	Model 2 (Auxiliary Plane?)
Nucleation latitude, deg	46.10 ± 0.02	46.10 ± 0.02
Nucleation longitude, deg	12.48 ± 0.03	12.48 ± 0.03
Depth, km	15.3 ± 1.4	15.4 ± 1.6
Length L_1, along-strike, km	16.7	2.4
Length L_2, antistrike, km	2.9	17.4
Strike angle, deg	238 ± 10 (auxiliary: **61**)	**62** ± 13
Dip angle, deg	47 ± 4 (auxiliary: **43**)	**42** ± 4
Rake angle,[a] deg	88 ± 4 (auxiliary: **92**)	**92** ± 5
Mach number$_1$, along-strike	0.84 ± 0.02	0.64 ± 0.05
Mach number$_2$, antistrike	0.65 ± 0.04	0.84 ± 0.04
V_S, km s^{-1}	3.75 ± 0.11	3.79 ± 0.10
M_0 10^{25} dyne cm	3.23 ± 0.3	3.31 ± 1.01
$\sum \mathbf{r}_s^2$	56	56

[a]With an ambiguity of ±180°, see text.

lations will be frustrated and will not reach any solution; if D is too low, all subpopulations will converge toward the same depression of the hypersurface of the residuals but will often be unable to catch the best solution. Our source population evolves starting with four subpopulations of 2000 sources. Our minima, corresponding to model 1 and model 2 in Table 2, were reached after 706 generations of sources.

3. Intensity Data

3.1. Site Effects

[20] Before performing the inversions we searched for site effects on the intensities. It is worth stressing, however, that intensity I does not refer to a very local site as does the location of a strong motion recording instrument, for example, whose seismic response is often very site-dependent. Rather, each I observation refers to a relatively large area (typically, one town or village) with nonhomogeneous site conditions. In previous papers we showed that these kinds of I values were rather independent from the site geology prevalent in each area. This held for both one Californian and one Italian catalog (see the relevant analysis in Tables III and IV of *Sirovich et al.* [2001] and of *Sirovich and Pettenati* [2001], respectively). We explained this by recalling that the very local behavior of a single building is swamped by the hundreds, or thousands, of buildings that provide the classification of each I degree for each town.

[21] For the study case, after discarding four sites classified as "felt," we searched for the statistical outliers in the remaining set of 263 data with I from IV to IX; for this we applied the classical Chauvenet method [*Barnett and Lewis*, 1978, pp. 19–20; see also *Johnston*, 1996], but no outliers were found in this way. Even the IV degree at Cordignano is compatible with the lognormal distribution of its class (IV) of distances from the source.

[22] A homogeneous soil classification is available for 124 sites of the Friuli-Venezia Giulia [*Carulli et al.*, 2002] and eastern Veneto (A. Zanferrari, written communication, 2003) regions, i.e., at epicentral distances of <113 km. These authors classified these territories into "rock," "stiff," and "soft" soil areas according to *Ambraseys et al.* [1996] and stored the information in a geographical information system (GIS) (A. Zanferrari, written communication, 2003). From this we extracted the soil classifications corresponding to the geographical coordinates of the sites given by G. Monachesi and M. Stucchi (unpublished data, 1997) in the DOM4.1 catalog.

[23] Unfortunately, the data set is not sufficient to draw statistical conclusions about the influence of the nature of the sites on their response in terms of damage and intensity, which is why we do not show any relevant figures. We only state that when the IV–IX intensity range is considered, the difference between the intensity/distance regressions related to "stiff" and "soft" sites are statistically insignificant. However, the regression plots of "rock" and "soft" sites are at the limit of the 95% confidence interval, respectively. However, there are only 10 sites in the IV intensity class and 6 sites in class IX. So, if the better-sampled V–VIII range is examined, the regressions of rocky and stiff sites almost coincide, while the difference with soft sites is only slightly significant from a statistical viewpoint for low intensities only (relatively higher distances). Thus we treated the data with no geological corrections. This, however, also agrees with the source inversion results of the Whittier Narrows earthquake of 1987 by *Zeng et al.* [1993, p. 371], who "did not find significant improvement or change between the results with and without this site effect correction. . .."

[24] The scarce relevance of the site characteristics on regional intensity patterns in the study case does not necessarily contradict other known evidence regarding local amplifications of macroseismic intensity. We also presented a case history of small microzones, in towns and hamlets struck by an earthquake in southern Italy, which experienced amplifications and deamplifications of 1–3 I units [*Siro*, 1982]. However, these peculiar seismic responses were associated with peculiar geomorphological, geotechnical, and geophysical characteristics of the various microzones within the studied sites.

3.2. Regional Patterns

[25] The distribution of the damage caused by this earthquake, tessellated with Voronoi polygons [*Pettenati et al.*, 1999; *Okabe et al.*, 2000], is in Figure 2. The dots in the figure are the sites that refer to the intensities, which are the same used for the inversions presented in this paper. The data shown come from the DOM4.1 catalog (G. Monachesi and M. Stucchi, unpublished data, 1997). However, the original data came from *Barbano et al.* [1986].

Table 3. Reference Source Parameters of the Bosco Cansiglio, 1936 Earthquake

Bibliographical Reference	Latitude, deg	Longitude, deg	Hypo Depth, km	Magnitude	Strike, deg	Dip, deg	Rake, deg
Barbano et al. [1986]	. . .	. . .	7–10[a]	5.2–5.9[b]	. . .	. . .	. . .
			15–20[c]	5.6[d]			
			15[d]				
NT4.1 (R. Camassi and M. Stucchi, unpublished data, 1997)	46.067	12.367	. . .	5.80 ± 0.35[e]	. . .	. . .	. . .
				6.2[f]			
CFTI [*Boschi et al.*, 1995]	46.05	12.42	. . .	6.1[g]	. . .	. . .	. . .
CPTI [*Boschi et al.*, 1999]	46.088[h]	12.380[h]	. . .	5.8–6.1[i]	. . .	. . .	. . .
				5.8 ± 0.7[e]			
Renner [2000]	46.100[h]	12.460[h]	17	5.8	230	45	56
Valensise and Pantosti [2001][j]	. . .[k]	. . .[k]	1.0–6.6[l]	. . .[m]	230	50	64

[a]According to the *Sponheuer* [1960] formula, with meizoseismal area of IX degree.
[b]So-called macroseismic magnitude, according to the approaches suggested by various authors [see *Barbano et al.*, 1986].
[c]As in footnote a, with the VIII degree meizoseismal area.
[d]Instrumental M_s and depth [see *Barbano et al.*, 1986].
[e]Instrumental M_s.
[f]Macroseismic.
[g]M_e (macroseismic); see definition by *Boschi et al.* [1995, p. 94].
[h]Instrumental.
[i]From the macroseismic data by *Barbano et al.* [1986], using the approaches suggested by various authors [see *Boschi et al.*, 1999].
[j]Mainly on geological evidence.
[k]They do not define an epicenter inside the extended fault source.
[l]Minimum and maximum estimated depth of the fault source.
[m]Estimated length, 12 km; estimated width, 7.3 km.

[26] *Barbano et al.* [1986] provided information for ~270 localities in the MCS [*Sieberg*, 1930] scale and also classified the reliability of the macroseismic information at the individual site by means of a weight from 1 to 4 (1 = very good; 2 = good; 3 = poor, and 4 signifies "no news was found," so the intensity was taken from other workers).

[27] There are two separate small groups of sites in Figure 2 where damage of the IX intensity degree was observed; the two groups are ~20 km apart. Consider, too, that the use of the Voronoi polygons in the figure helps us to understand the information density and, above all, continuity. This is a clear sign that one is not allowed to include these two groups of IX degree sites in a continuous meizoseimal area because several polygons of degree VIII exist in between. As regards the noteworthy presence of two areas of maximum intensity IX, it must be highlighted that (1) the reliability of the intensity determinations in those sites goes, according to *Barbano et al.* [1986] (see section 6.2), from "very good" to "good" and that (2) one area is in the mountainous region close to the instrumental epicenter, and the other is in the piedmont zone (see Figure 2). For this situation, *Barbano et al.* [1986] hypothesized either site effects in the piedmont zone or a source effect. In the former hypothesis the meizoseismal area would be the northern one. In the latter the so-called macroseismic epicenter, i.e., the baricenter of highest intensities, would lie in between.

[28] Coming back to the search for site effects of section 3.1 and to the two areas of intensity IX (see Figure 2), it is worth noting that the three southern sites are "soft," but, as seen before, the difference between rocky and stiff sites on the one side, and soft sites on the other, has no statistical significance for high intensities. Thus there is no proof of amplification; the lack of apparent amplification could be due to the effects of soil nonlinearity.

[29] In the following we redetermine the epicenter from the intensity inversions and show that a source effect can be invoked for the aforementioned duplication of the area of maximum intensity IX. The previous intensity of the IV degree, reported by DOM4.1 at Cordignano, on the border between the areas of the VIII and IX degree (see the anomalous white polygon in Figure 2), is worth commenting on. We know from the original study by *Barbano et al.* [1986] that Cordignano experienced an intensity of the VII degree. Unfortunately, though, the IV degree is a typing error by DOM4.1. However, we kept the wrong datum to maintain our standard approach of using data from available catalogs.

[30] Figure 2 shows more characteristic features: see, for example, the abrupt passage from VIII to V to the north and from VII to V to the south, probably due to the insufficient sampling there. Also, see that the area of the VII degree appears to extend toward ESE. According to traditional empirical practice, this would be interpreted in terms of lower "attenuation" in that direction. A source effect can also be invoked, as will be seen in section 6.

4. Reference Source Parameters

[31] Table 3 presents the reference source parameters available for the Bosco Cansiglio, 1936 earthquake before this study; they came from (1) macroseismic intensities I, (2) early instrumental recordings according to traditional seismological practice, and (3) combined geological and geophysical evidence. Consider that the so-called macroseismic magnitudes were roughly calculated from intensity (see the mentioned papers). There is a considerable uncertainty in the magnitude determination of the study earthquake (from 5.2 to 6.2) to be noted. The epicenter locations contained in the more recent consensus parametric catalog CPTI [*Boschi et al.*, 1999] were determined using the *Gasperini et al.* [1999] technique.

[32] *Renner* [2000] revised his previous hypocentral location and focal mechanism [*Slejko et al.*, 1987, 1989] obtained from the signs of the first pulses of the early

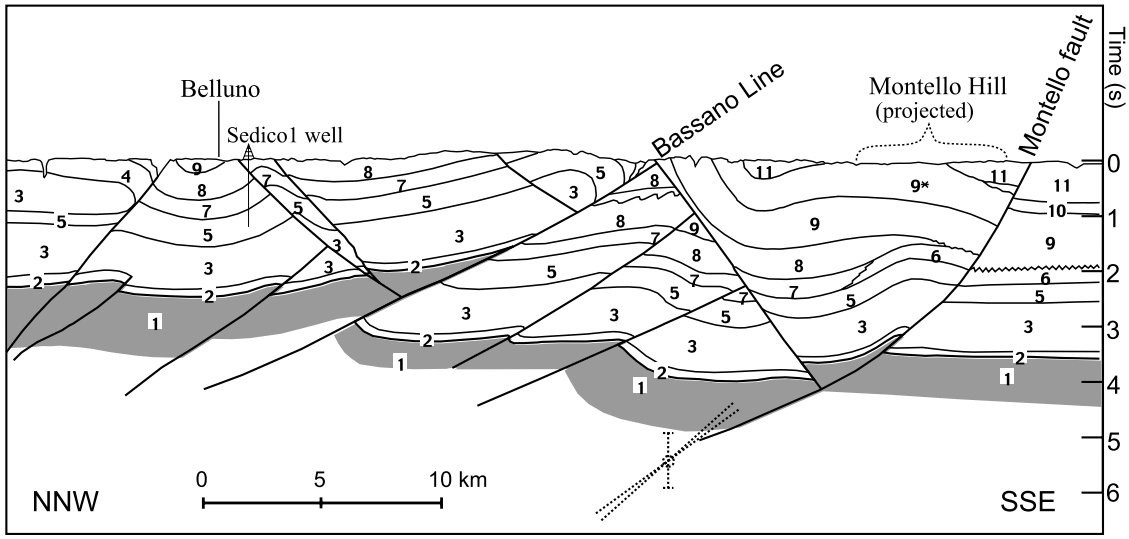

Figure 4. Interpretation of the migrated section of the southern TRANSALP segment from the chain (left) to the Italian foreland basin (right). The vertical scale of the two-way time section is in seconds. Symbols are as follows: 1, metamorphic basement; 2, Permian; 3, Triassic (undifferentiated); 4, upper Triassic; 5, Jurassic; 6, Cretaceous (carbonatic platform); 7, Cretaceous (basinal deposits); 8, Eocene Flysch; 9, Neogene molasses (9* in the upper part refers to the Messinian Conglomerates); 10, Marine Pliocene; 11, Plio-Pleistocene-Holocene [modified from *Bertelli et al.*, 2003].

instrumental recordings, making a total of 38 polarities available. His epicenter of the Cansiglio, 1936 earthquake is approximately 8 km WNW of the macroseismic epicenters (see star number 3 in Figure 1). His minimum variance model is a dip-slip mechanism (which scores 36 correct signs over 38); however, a strike-slip solution is compatible with 35 readings. Finally, source number 124 from the database of potential sources in Italy by *Valensise and Pantosti* [2001, p. 908] relates to the Bosco Cansiglio, 1936 earthquake. As shown in Table 3, their reference source parameters came mainly from the respective orientations of (1) the maximum horizontal geodynamical compressive stress (NNW-SSE) and (2) the tentative rupture plane, which was hypothesized from the position of the Aviano Overthrust southeast of the instrumental epicenter (P. Burrato, personal communication, 2003).

5. Seismotectonic Outline

5.1. Alpine Context

[33] At a regional scale the study area is generally interpreted within the indenter tectonics interaction between the European plate on the northern side and the Adriatic and African plate to the south. At a more local scale (see Figure 1) the piedmont line is characterized by the presence of the external front of the chain shortened by compression; the most important tectonic features of this southern part of the Southern Alps are two principal adjacent lines: (1) the so-called Bassano-Valdobbiadene, or, simply, Bassano Line (as by *Doglioni* [1990]) to the west and (2) the Maniago Line [*Doglioni*, 1990] alias the Aviano segmented Overthrust to the east [*Beinat et al.*, 1988; F. Galadini and P. Messina, unpublished manuscript, 2001). The connection between these two lines is controversial: the ridge shape of the mountainous front, SSW of the Santa Croce Lake (see Figure 1), could suggest a continuation of the Bassano Line toward the NNE [*Ambrosetti et al.*, 1983; *Castaldini and Panizza*, 1991]; eastward, the promontory-shaped southernmost part of the Cansiglio Plateau is a morphotectonic escarpment [*Zanferrari et al.*, 1982]. In this context a dextral transpressive transfer zone connecting the Bassano Line to the Maniago Line (as by *Doglioni* [1990]) or a reverse fault (as by *Ambrosetti et al.* [1983]) could be suggested; we put a question mark on it in Figure 1. Also, note that in this controversial northwest-southeast oriented structure the Col Visentin normal fault is found northwest of it (C.V. in the figure [from *Pellegrini and Zanferrari*, 1980]). In Figure 1, for the Aviano Overthrust, we follow the segmentation proposed by F. Galadini and P. Messina (unpublished manuscript, 2001); the segments are sketched by solid lines. In actual fact the overthrusted front is composed of a series of tectonic wedges arranged in an imbricate fan geometry; the wedges were formed in later stages, from the Cretaceous onward, and the most recently formed wedges generally lie at the front, where the present activity seems to be concentrated [see *Beinat et al.*, 1988]. These wedges go from some hundreds of meters to some kilometers wide and are delimited by faults having various directions, but more often, WSW-ENE trending and dipping toward the NNW [*Beinat et al.*, 1988]. We cannot go into detail about this here, but for a recent collection of tectonic interpretations of the area the reader can refer to *Anonymous* [2003].

[34] The Montello growing ramp anticline in Figure 1 is worth noting. It is generally interpreted as a propagating fold moved by an inverse fault, for which a vertical uplift rate of 1 mm yr^{-1} after 121 ka has been estimated [*Benedetti et al.*, 2000]. Note that in this structure (1) the Montello fault is aligned with the Aviano segmented Overthrust and (2) the River Piave and its affluent, in the southwest corner of the figure, were clearly diverted by

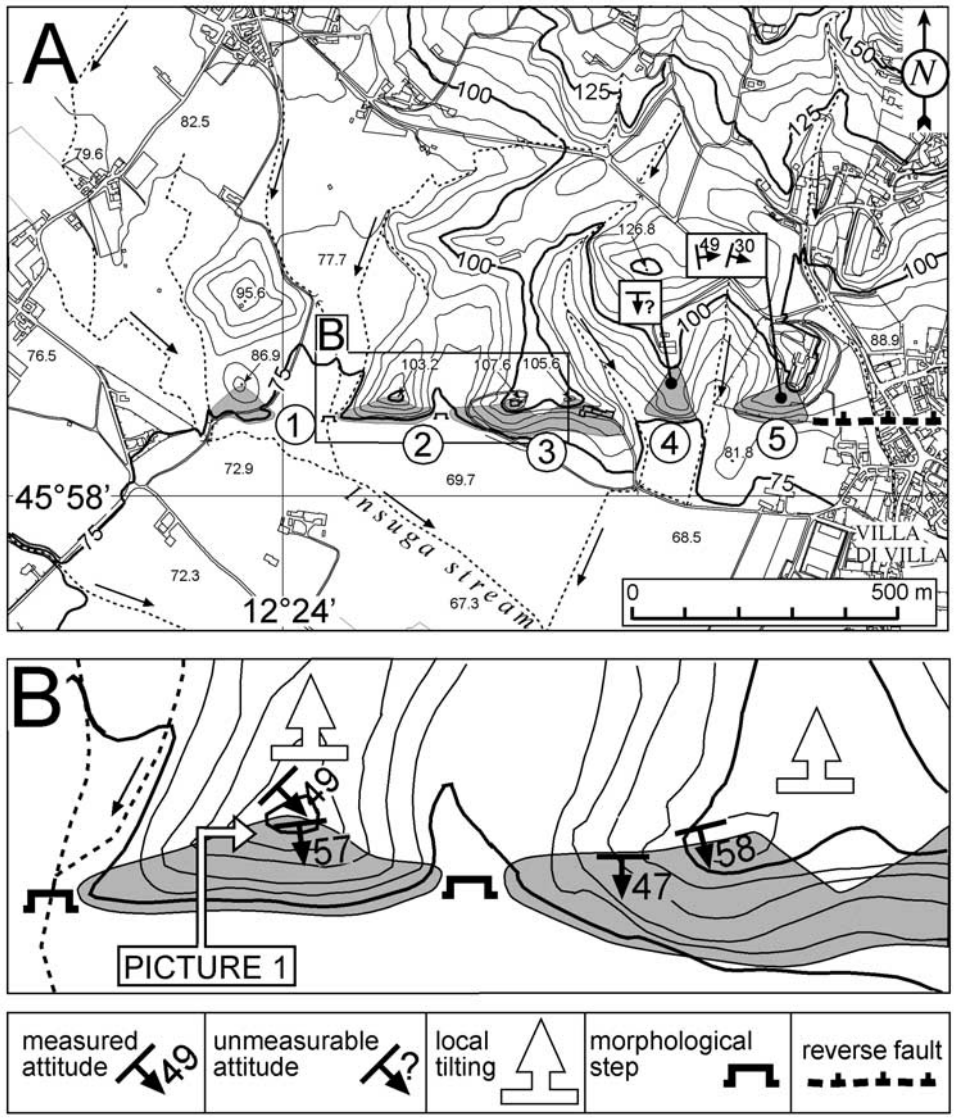

Figure 5. Geological, morphological, and neotectonic sketch of one part of the complex Aviano Overthrust near Villa Di Villa [modified from *Soramel and Zaia*, 1985] (courtesy of A. Zanferrari).

the uprising of the Montello Hill. However, also note that the Monticano Stream was not diverted, suggesting a discontinuity between the Montello segment and the Aviano Overthrust.

[35] Figure 4 shows the southern part of the interpreted migrated TRANSALP section from the Southern Alps chain to the Veneto Plain (to the right of the figure, SSE) recently produced by *Bertelli et al.* [2003]; see the tectonic structure of the area, and note that these authors think that the Bassano Line (called the "Flessura Pedemontana Overthrust" in their original figure) strongly displaced the basement but also that the front of the Montello thrust reached it. For the hypothetical relation between the deep structure of the epicentral area of the study earthquake and that of Figure 4, as well as for the projection of our source on this section, see section 7.

[36] The knowledge of the neotectonics in this area is still generally at a preliminary stage. Some interesting information about the southernmost, promontory-shaped flank of the Cansiglio Plateau comes from an unpublished thesis by two students of A. Zanferrari of Padua University [*Soramel and Zaia*, 1985] (courtesy of A. Zanferrari; see section 5.2). From the above-mentioned thesis we discovered that the southernmost front of the Aviano Overthrust is interpreted to override sediments of Miocene, upper Pleistocene, to Holocene age. In fact, along this front, on the southern flank of the Plateau, some likely morphoneotectonic evidence is encountered, such as some deformed late Glacial to Holocene deposits and morphologies; this implies recent, perhaps still active, movements of the complex overthrust.

5.2. Intriguing Neotectonic Signs

[37] To introduce the inversion results that follow, the information in Figures 5 and 6 [after *Soramel and Zaia*, 1985] should be considered; they exemplify two likely near-fault morphoneotectonic signs, which are compatible with the source retrieved in the present study (see sections 6.2 and 7.2).

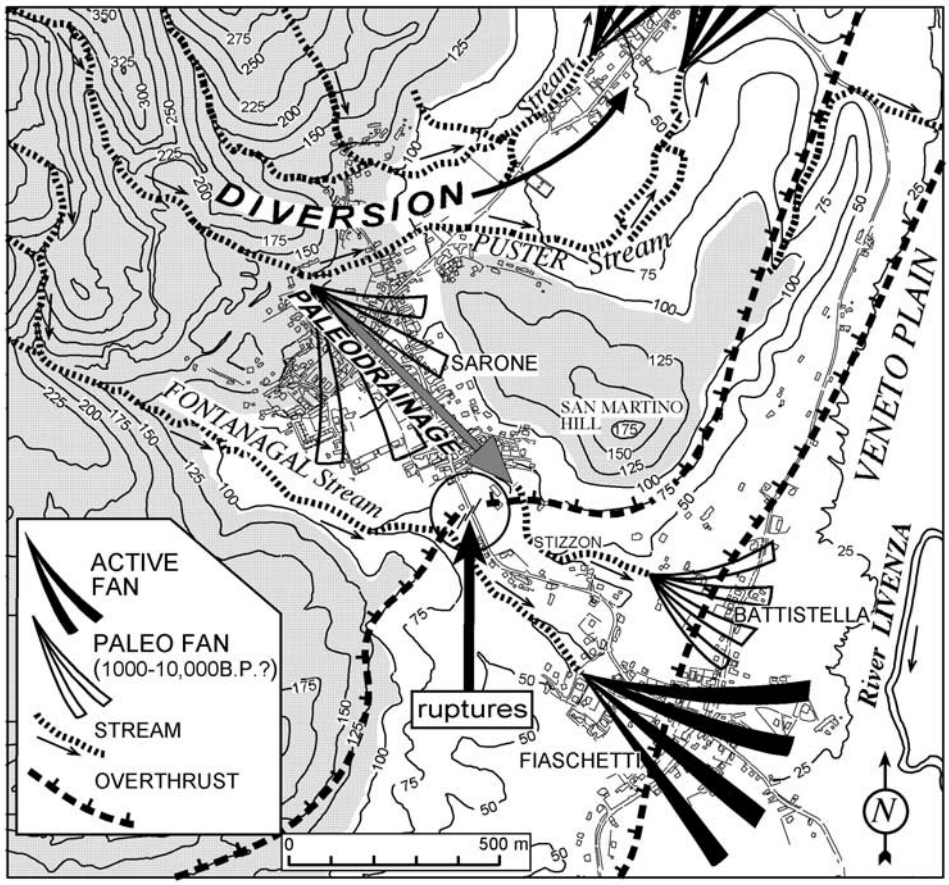

Figure 6. Geomorphological and neotectonic sketch of one part of the complex Aviano Overthrust near Fiaschetti [modified from *Soramel and Zaia*, 1985] (courtesy of A. Zanferrari). See the tentative position of the 1936 rupture found by *Andreotti* [1937] inside the circle indicated by the arrow.

[38] Figure 5a shows an area immediately west of the village of Villa Di Villa. Here, four triangular facets (numbers 2–5 in Figure 5a, whereas number 1 is doubtful) and two morphological steps in the plain (see Figures 5a and 5b) are aligned with the trace of an east-west oriented, north dipping reverse fault. This fault is a subsidiary of the complex Aviano Overthrust; its trace is a dashed line on the right-hand side of Figure 5a. Note that the minor tectonic wedges of the front of the Aviano Overthrust, on the southern flank of the Cansiglio Plateau, often cause direct contact between the Monte Cavallo limestone (Malm, upper Cretaceous) to the north and the Montello Formation (which is a sequence of siltites and sandy clays, with interbedded lenses of conglomerate) to the south. At most, an upper Miocene, or more probably a younger age, was hypothesized for the conglomerates [*Soramel and Zaia*, 1985]. Noteworthy is the fact that recently, the upper part of the Montello conglomerates, which constitute the hilltops 1–5, were called unit 3, and a late Pliocene–early(middle?) Pleistocene age was hypothesized for them [*Caputo et al.*, 2003]. See their attitude and their alluvial origin in Figure 7 (picture taken on hilltop number 2). Furthermore, the north facing crests descending from hilltops number 2–3 in Figure 5a are formed by the fine facies of the Montello Formation. Note in particular that (1) the conglomeratic strata on hilltops 2–3 dip southward, while (2) those on hilltop 5 dip eastward, and (3) the attitude of those on hilltop 4 is chaotic. This suggests that the triangular facets west of Villa Di Villa are controlled by the presence of the east-west segment of the Aviano Overthrust, shown on the right-hand side of Figure 5a. Consider that the western morphological step, previously mentioned and shown in Figure 5b, dislocated the bottom of a stone-paved canal, which was built some 50–100 or more years before present, and is ~0.8 m high. The eastern step marks the southern limit of a north-south trending, 250-m-long hanging valley, partly filled with colluvial-alluvial fine sediments eroded from the Montello Formation, and is ~1.8 m high. Incidentally, in Figure 5 the northward facing crests descending from hilltops number 2–3 could suggest some back tilting (large open arrows in Figure 5b). To conclude our comments on Figure 5, it appears unlikely that the simultaneous presence of these diverse signs would be haphazard, so we tend to interpret them as landforms associated with the present propagation of the inverse fault seen in Figure 5a, with tilting.

[39] An even more evident neotectonic symptom is shown in Figure 6 (see its location in Figure 1). This figure presents the geomorphological environment where Andreotti found a coseismic rupture in 1936 [*Andreotti*, 1937]. We recall that the earthquake occurred on 18 October 1936 at 0310:53.6 UT. *Andreotti* [1937, p. 10–11] writes

Figure 7. Conglomeratic strata of the so-called Montello Formation outcropping on hilltop number 2 of Figure 5b (the picture was taken from the west; each colour on the graduated topographic rod is 20 cm high).

that on 17 October at ~1900 UT (thus 8 hours before the earthquake),

> ...a series of ground ruptures opened at the Stizzon hamlet, along the Sarone-Fiaschetti [unpaved] road. The trend of these ruptures was NNE-SSW, and they were aligned with the San Martino Hill; they were each 3 m long and 0.5 cm wide. Just after the shock, they found the ruptures increased to approximately 1 cm....

(The hypothesized location of the ruptures is encircled in the central zone of Figure 6.) Figure 6 shows that (1) the overthrust mapped by *Soramel and Zaia* [1985] crosses the Sarone-Battistella road just in the northern part of the hamlet of Stizzon and that (2) the greater mass of the San Martino Hill is just ENE of this intersection. Perhaps a rupture setting en echelòn could be evoked in the direction of the ground ruptures (''NNE-SSW'' according to *Andreotti* [1937, p. 11]) by this minor discrepancy. The ruptures encircled in Figure 6 are drawn following the en echelòn hypothesis and are not to scale. The plane of the overthrust is almost horizontal, east of the broken road, while west of it, the dip is WNW. Moreover, two intriguing diversions of streams are found in the area, which could be caused by a recent uplift of the Aviano Overthrust shown in the figure. Looking at the two alluvial fans in the lower right-hand corner of the figure, it can be seen that they span across the Fiaschetti and the Battistella hamlets. The former fan is still fed by the Fontanagal Stream (strictly speaking, it was still fed before some recent canals were built), while the latter is no longer fed by the Puster Stream. In fact, after the last glaciation this stream was naturally diverted toward the northeast. Before being diverted 1 to 10(?) ka this stream also flowed through the area where the Sarone village is now located (see the direction of the ''paleo-drainage'' in Figure 6). In the figure we also highlighted all the areas that are above an altitude of 105 m with a veil. In this way, the morphology shown in the figure is clearer, and the diversion of the Puster Stream, and of another, anonymous stream, in the upper part of the figure is more noticeable. Concluding the examination of Figure 6, there is evidence of neotectonic, and also coseismic, activity in this part of the complex external front of the Aviano Overthrust.

6. Results

[40] First, we explored the hypersurface of the residuals with the grid search technique, but since this search is extremely time consuming, we did a quick search adopting a symmetric source, with larger incremental variations of the source parameters than in Table 1. In doing so, we obtained a preliminary minimum variance model with a $\sum \mathbf{r}_s^2 = 85$. Apart from the symmetry of this source, the other focal parameters of the 1936 earthquake were in agreement with those automatically found by the NGA, with a difference of 24° in the rake angle.

[41] The NGA algorithm identifies two absolute minima in the multiparameter space both for $\sum \mathbf{r}_s^2 = 56$ and for the same hypocenter (46.10° ± 0.02°, 12.48° ± 0.03°, depth of 15.3 ± 1.4 and 15.4 ± 1.6 km, respectively). These two minimum variance models are shown in Table 2. The table reports the source parameters with their estimated errors.

[42] The tessellated synthetic pseudointensities produced by model 1 of Table 2 are in Figure 8. The inset shows the fault plane solution corresponding to model 1. Comparing Figures 2 and 8, it can be seen (1) that the two meizoseismal

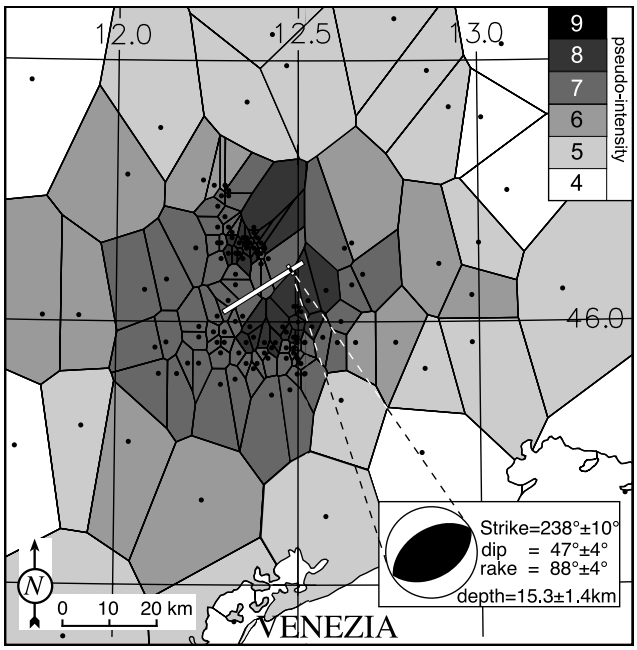

Figure 8. Tessellated synthetic pseudo-intensities produced by model 1 of Table 2, retrieved by automatically inverting the observed regional intensity pattern. The inset shows the fault plane solution corresponding to model 1.

areas are in both of them and (2) the noteworthy similarity of the areas of degrees VII and V.

6.1. Errors

[43] Field intensity observations from several independent researchers were not available. For this reason we calculated the inversion errors with the bootstrap technique [*Press et al.*, 1992, p. 684–687], repeating the procedure by *Pettenati and Sirovich* [2003, p. 55] to the letter. Errors in Table 2 refer to one standard deviation as by *Pettenati and Sirovich* [2003, p. 55, last paragraph, and Table 3]. Incidentally, we think that given the half-space medium assumption, hypocentral depth is poorly determined.

6.2. Best-Fitting Model and Its Context

[44] Model 1 of Table 2 (second column) is, supposedly, the rupture plane; this hypothesis is based on the seismotectonic context and on neotectonic evidence (see Figures 1, 5, and 6). Model 2 is very close to the auxiliary plane of model 1 in the fault plane solution. The strike, dip, and rake angles of the theoretical auxiliary plane of model 1 in the fault plane solution can be seen in parentheses (bold numbers) in column 2. Both models 1 and 2 have almost pure dip-slip mechanisms (as said, pure dip-slip mechanisms imply perfect bimodality).

[45] See the theoretical radiations, in terms of *KF* dimensionless values from equations (1) and (2) of *Pettenati and Sirovich* [2003], of the models 1 and 2 in Figures 9a and 9b, respectively. Note their strong resemblance. For the reader's convenience, in Figure 9 we reported the fault plane solutions and the central values of the source parameters of models 1 and 2 of Table 2. In particular, note that in Figure 9 (and Table 2) (1) the hypocentral coordinates, the seismic moments, and the half-space V_S retrieved for the two models coincide, or almost coincide (see the horizontal relation segments in the figure) and that (2) the along-strike and antistrike rupture lengths (L_1 and L_2) and Mach numbers are almost perfectly specular (see the cross-arrow relations in the figure).

[46] Figure 10 presents model 1 of Table 2 in its seismotectonic context. In the figure the thick segment in white, striking from WSW to ENE shown in the center of the area, is the vertical projection of the line source of model 1. Recall that our line source is a plane of unit width, and note the asymmetric position of the epicenter (marked by the small black square) running along it. In the figure we also virtually prolonged this rupture plane to the surface of the Veneto Plain, according to its angle of dip; in this way the black dashed segment is obtained, which represents the virtual intersection between the central solution of the rupture plane model 1 and the plain. Theoretically, then, once the errors of the inverted strike angle [238° ± 10°], dip angle [47° ± 4°], depth [15.3 ± 1.4 km], latitude [46.10° ± 0.02°], and longitude [12.48° ± 0.03°] have been accounted for, this virtual intersection could lie anywhere within the approximately saddle-shaped sector of the piedmont plain patterned in black in the figure. However, we think that the actual intersection between the source and the plain (if any) should be found a little more to the northwest, where the sector patterned in white is drawn in the figure (see section 7 and its discussion on the seismotectonic interpretation). Finally, Figure 1 shows that the inverted epicenter was moved from the area of the macroseismic epicenters to the location of the instrumental location by *Slejko et al.* [1989] (which is confirmed by *Renner* [2000]).

[47] We repeated our source inversion also by adopting $\sum_q^1 r_s^2$ as the fitness criterion, where q subjectively quantifies the aforementioned reliability of the data by *Barbano et al.* [1986]. In the absence of any quantitative criteria for the choice of the weight we adopted the following q values: q = 10 for "very good"; q = 15 for "good"; q = 20 for "poor"; q = 25 for "no news." *Barbano et al.* [1986] also rated the reliability of intermediate intensity degrees on a scale from 1 to 4, such as VI–VII. In this respect, recall that VI–VII means not lower than VI and not higher than VII; in these cases we obeyed the "poor" and "no news" reliability by these authors, while we degraded the few cases of "very good" or "good" to q = 18. The choice of these weights was made a priori, and no adjustments were subsequently made. Finally, we also recall that reliability in general is "very good" to "good" in the two meizoseismal areas and "no news" in the peripheral sites of Figure 2 (the figure of the geographical distribution of the reliability is not shown here).

[48] The NGA inversion with $\sum_q^1 r_s^2$ was rather sensitive to the subpopulation distance D (equation (1)) so that the best subpopulation converged toward the hypothesized rupture plane or, alternatively, toward its auxiliary plane. See the two best solutions achieved in Table 4. In this case the hypocenters of the two solutions are close to each other but not coincident. Also note that the lowest value for $\sum_q^1 r_s^2$ corresponds to the rupture plane striking southwest and dipping northwest ($\sum \mathbf{r}_s^2 = 55$, $D = 0.0842$), but for $D = 0.0820$ the best subpopulation converges

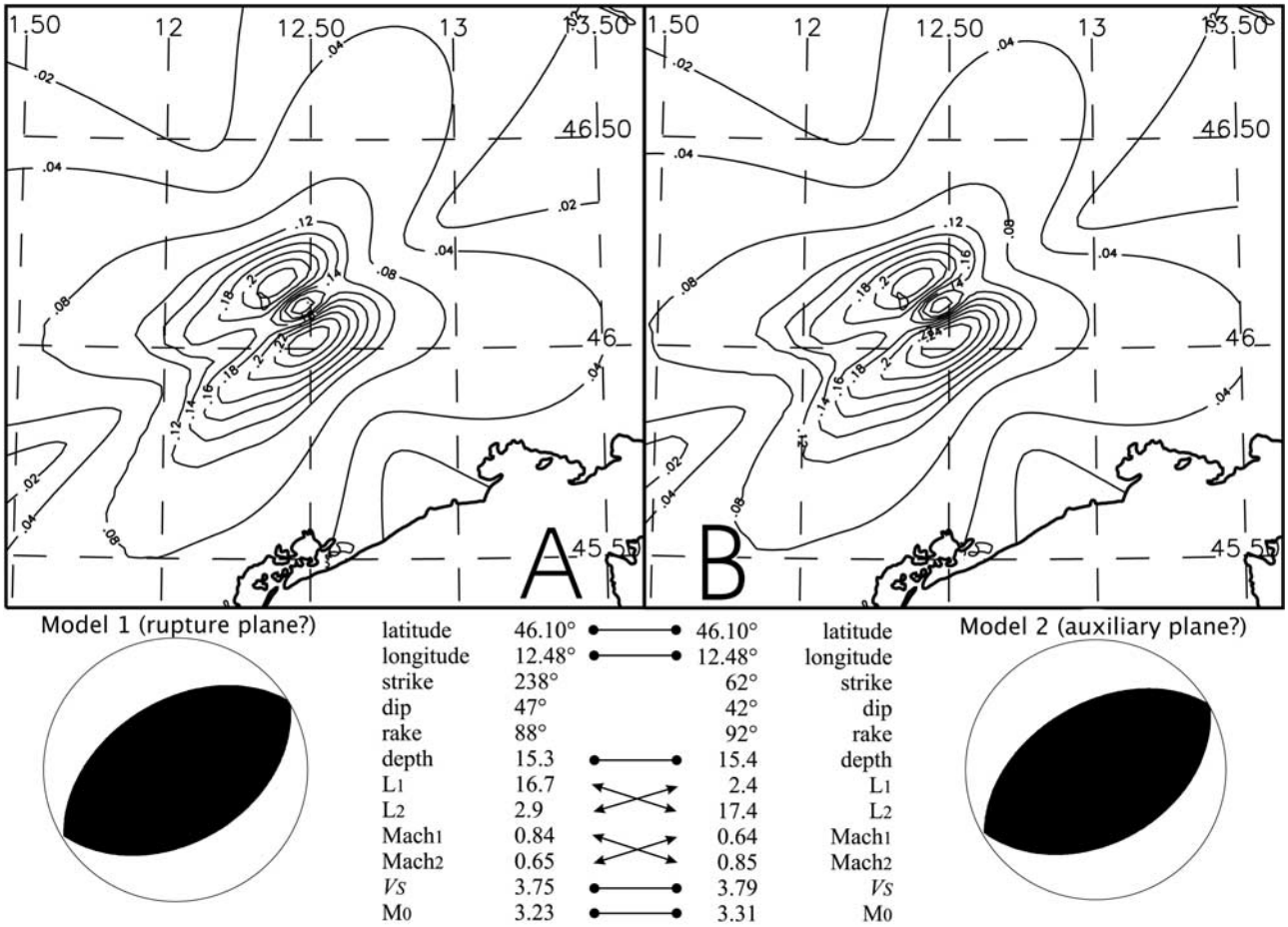

Figure 9. (a) Theoretical pseudo-intensity radiation of model 1 of Table 2 (supposedly, the rupture plane). (b) The same as in Figure 9a for model 2 (which is close to the auxiliary plane of model 1). See Table 2 and text.

toward the hypothesized auxiliary plane striking ENE (with $\sum \mathbf{r}_s^2 = 59$).

7. Discussion

7.1. Bimodality

[49] *Koper et al.* [1999] had already shown bimodality in the seismological inversion of fault plane solutions, but we did a considerable amount of work before understanding that in our more complicated model the ambiguity between the two auxiliary planes increases the closer the rake angle is to 90° (±180°) and, secondarily, the more the rupture is symmetric [*Pettenati and Sirovich*, 2003]. Thus the matter of bimodality in our inversions deserves a comment. We quantified the degree of bimodality in terms of

$$\text{mean residual} = \frac{\sum_{i=1}^{400} |I_{\text{RP}} - I_{\text{AUX}}|}{400}, \qquad (2)$$

where, I_{RP} is the pseudo-intensity (in integer numbers), synthesized at every node of a 20 × 20 regular grid, over the study area of Figure 1; I_{RP} is synthesized by using a series of sources, which start from model 1 in Table 2 and explore the whole ranges of the dip and rake angles and the 0.5–1.0 range of the Mach number, one parameter at a time. RP stands for rupture plane. Then, I_{AUX} are the corresponding values obtained by using the theoretical auxiliary planes in the fault plane solutions. In other words, we express bimodality as the mean residuals of intensity between the rupture plane and its auxiliary plane over the grid; mean residual = 0 means perfect ambiguity between the pseudo-intensities radiated by the two planes. Figure 11a shows the aforementioned mean residual of equation (2) over the rake angle. As seen, mean residual = 0 (perfect bimodality) only holds for the rake = 90° (±180°).

[50] Then, Figures 11b and 11c do the same for the dip angle and the Mach number, respectively (the rake angle is 88°). As seen from these figures, and keeping the other source parameters of model 1 of Table 2 fixed, the mean residual slowly increases with increasing dip angle (Figure 11b) or with increasing Mach numbers (Figure 11c). Thus given the almost bimodal model 1, a dip angle close to 90°, or a Mach number close to 1, would be needed to render the inversion problem unambiguous. In other words,

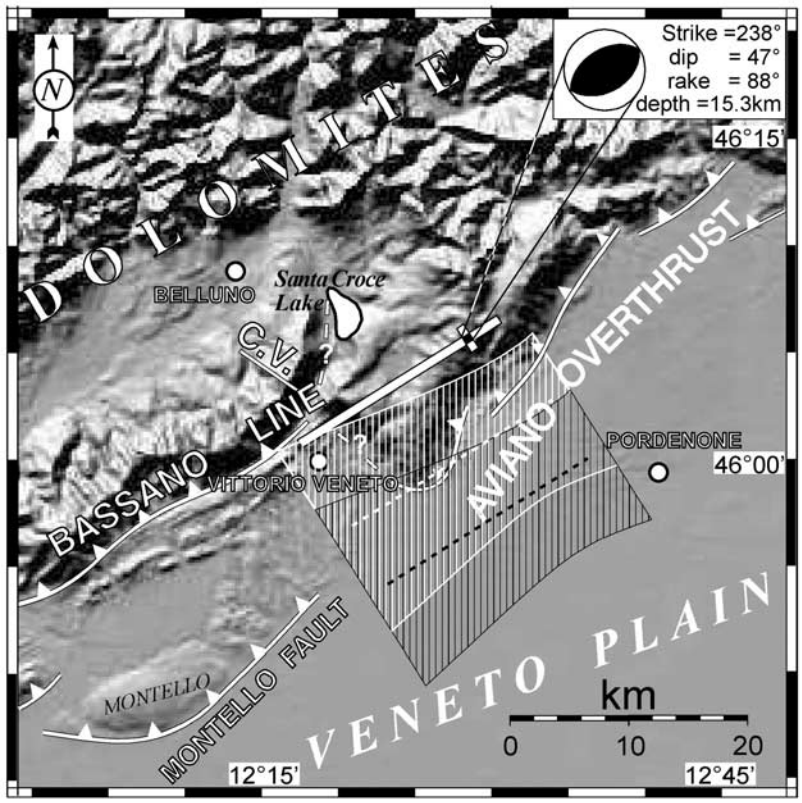

Figure 10. Same as in Figure 1. The two-patterned, saddle-shaped, overlapping areas SSE of our line source show the sectors of the piedmont plain, adjacent to a segment of the Aviano Overthrust, where the virtual prolongation of the rupture plane of model 1 in Table 2 emerges (see text for information about both the black-patterned area and for the white one).

Figure 11 confirms that the study case (rake = 88°, dip = 47°, Mach number $\leq$ 0.84) is almost bimodal.

7.2. Seismotectonic Interpretation

[51] By comparing Tables 2 and 3 (and 4), one can see that the inverted rupture plane matches the one inferred by other methods. Models 1 in Tables 2 and 4 are also compatible with the NNW-SSE oriented maximum horizontal geodynamical compressive stress, which has been confidently and unanimously measured and interpreted [e.g., *Doglioni*, 1990; *Montone et al.*, 1996].

[52] Then, the saddle-shaped sector of the piedmont plain, shown with a white pattern in Figure 10, was obtained in the same way as the corresponding black-patterned sector in the figure but only after subjectively adopting a nucleation depth of 10 km. The reason for this subjective choice was

Table 4. As in Table 2, but After Weighting the Site Intensities According to the Reliability Classification That Was Given by *Barbano et al.* [1986][a]

Parameter	Model 1 (Rupture Plane?)	Model 2 (Auxiliary Plane?)
Nucleation latitude, deg	46.12 ± 0.02	46.09 ± 0.02
Nucleation longitude, deg	12.50 ± 0.04	12.45 ± 0.04
Depth H, km	14.9 ± 1.4	14.5 ± 1.6
Length L_1, along-strike, km	2.2	2.3
Length L_2, antistrike, km	17.6	8.8
Strike angle, deg	237 ± 8 (auxiliary: **67**)	**61** ± 17
Dip angle, deg	47 ± 4 (auxiliary: **43**)	**40** ± 4
Rake angle,[b] deg	83 ± 6 (auxiliary: **97**)	**89** ± 13
Mach number$_1$, along-strike	0.86 ± 0.04	0.70 ± 0.06
Mach number$_2$, antistrike	0.63 ± 0.05	0.80 ± 0.04
V_S, km s^{-1}	3.68 ± 0.28	3.69 ± 0.19
M_0, 10^{25} dyne cm	3.27 ± 0.71	3.80 ± 0.58
$\sum \frac{1}{q} r_s^2$	2.5044	2.4855
$\sum \mathbf{r}_s^2$	55	59
Distance D (equation (1))	0.0842	0.0820

[a]Fitness criterion is $\sum \frac{1}{q} r_s^2$ (see text).
[b]With an ambiguity of ±180°; see text.

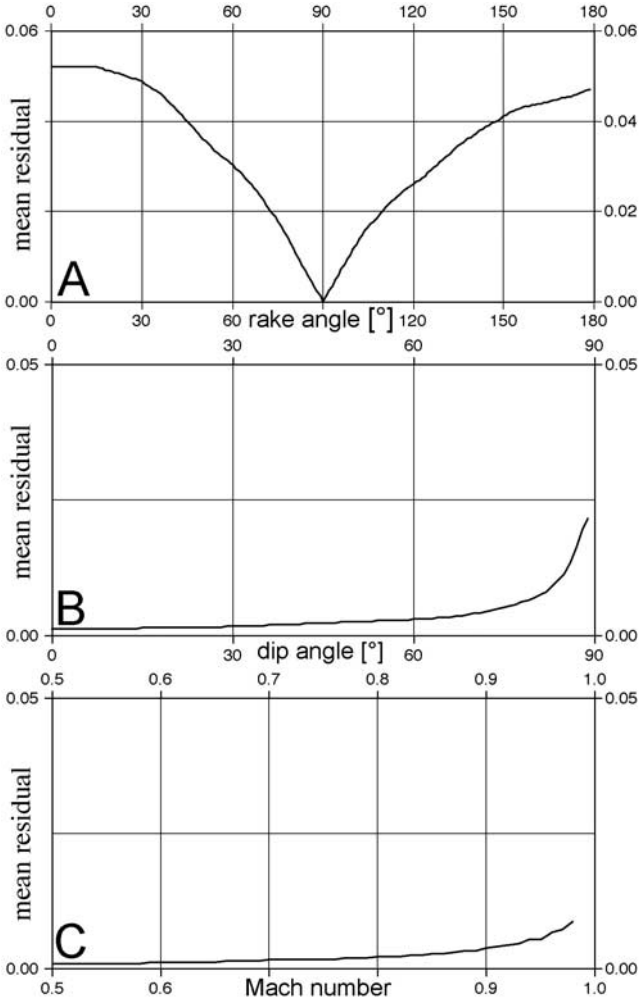

Figure 11. Variation of bimodality in the studied nonlinear problem. (a) Mean residual of equation (2) over the rake angle. (b) The same over the dip angle. (c) The same over the Mach number = V_r/V_S.

the following. Firstly, in most parts of the so-called Alpide Belt the hypocenters of earthquakes of comparable magnitude are a little smaller than 15 km [e.g., *Seeber et al.*, 1980; *Siro and Slejko*, 1982], and secondly, a listric shape of the overthrusts is plausible in this area, and therefore the virtual intersection between the upward prolongation of our model 1 rupture plane and the Veneto Plain could be closer to the piedmont line and to the Aviano Overthrust than the black-dashed segment in the figure (which is the intersection obtained from inversion).

[53] To project our model 1 of Table 2 on the section of Figure 4, we considered their orientations and adopted a mean *P* wave velocity of 5.5 km s^{-1}. The depth and the dip angle errors of our best solution are shown; the latitude error is not shown for simplicity, but remember from Table 2 that it is approximately a 2 km error. The depth retrieved by our inversions (14.9–15.3 (±1.4) km) is in notable agreement with the instrumental result by *Slejko et al.* [1989] (17 km); however, we are certainly aware that this is rather fortuitous given our half-space crustal model.

[54] We also stress that there are geometrical and tectonic reasons for handling the structure-source match of Figure 4 with caution. In fact, our rupture for the 1936 event (Figure 1) is 6–22 km ENE of the TRANSALP transect. Therefore, strictly speaking, to project it onto this section is arbitrary. Moreover, consider that the connection between the Bassano Line or the Montello fault, seen in Figure 4, and the Aviano Overthrust, seen in Figures 1 and 10, is controversial. Figure 4 shows, however, that our model 1 source is compatible with the general tectonic structure of the area, and Figure 10 suggests, quite strongly, that the study earthquake was provoked by one segment of the Aviano Overthrust. Also, consider that in 778 A.D. and in 1695 (see G. Monachesi and M. Stucchi, unpublished data, 1997) the Veneto Region was struck by two destructive earthquakes that still need to be tentatively associated to some causative sources.

[55] Concluding the discussion, a direct connection between our source models 1 of Tables 2 and 4 and the morphoneotectonic symptoms described in Figures 5 and 6 is not demonstrated. However, these symptoms are compatible with the source retrieved in the present study.

8. Conclusions

[56] In this work, and in the preceding one [*Pettenati and Sirovich*, 2003; *Gentile et al.*, 2004], we wanted to see if by treating the intensities in an innovative way, it is possible to catch the approximate geometric and kinematic characteristics of the sources of some destructive earthquakes. The comparison between our results of Table 2 (and also of Table 4) with the reference source parameters shown by Table 3 demonstrates that in the case of the Cansiglio, 1936 earthquake, automatic and fast source inversion is feasible. The use of four subpopulations of 2000 individuals led the NGA, rather rapidly, to a minimum variance solution, close to a preliminary solution already found by the grid search technique and with a better $\sum \mathbf{r}_s^2$. The NGA also found its auxiliary plane. In fact, the NGA let two subpopulations niche within the two principal depressions of the topography of the residuals.

[57] Both the NGA inversions of unweighted data and of weighted data converged more or less toward the same results, i.e., approximately toward the source parameters independently retrieved from different observations and data. We believe that our attempt of applying our new inversion technique to an earthquake of the early instrumental era was successful.

[58] Our study confirmed that bimodality causes a strong ambiguity when rake angles are close to 90° (±180°). Note that we obtained eleven source parameters by treating peculiar semiquantitative data alone, which is what intensities are.

[59] The present results confirm that the inversion of regional intensity patterns is, at least in some cases, a stable phenomenon. Furthermore, these results also encourage us to validate our inversion technique with more well-documented earthquakes and to treat preinstrumental earthquakes, which remain our principal target.

[60] From the seismotectonic viewpoint the inverted rupture plane of the 1936 Cansiglio earthquake is compatible with (1) the general tectonic structure of the area and, in particular, with (2) one outcropping segment of the complex Aviano Overthrust, which overrides sediments of Holocene

age and approximately marks the piedmont line of the Veneto Plain.

[61] **Acknowledgments.** This research was supported by the "Scenari di danno nell'area veneto-friulana" grant of the National Group for the Defense Against Earthquakes (GNDT) of the Istituto Nazionale di Geofisica e Vulcanologia (INGV). Thanks go to Adriano Zanferrari, of the University of Udine, for calling our attention to the physiographic features shown in Figures 5 and 6; thus the contents of these figures are taken, in part, from a thesis by *Soramel and Zaia* [1985] (courtesy of their tutor, A. Zanferrari) (possible errors in the two figures are ours). We are indebted to Carlo Bosi for critically reading paragraph 5.2 and Figures 5–7, to our colleague Francesco Gentile, who kindly set up the NGA code for us, and to the reviewer Julian Bommer.

References

Ambraseys, N. N., K. A. Simpson, and J. J. Bommer (1996), Prediction of horizontal response spectra in Europe, *Earth Eng. Struct. Dyn.*, *25*, 371–400.

Ambrosetti, P., C. Bosi, F. Carraro, N. Ciaranfi, M. Panizza, G. Papani, L. Vezzani, and A. Zanferrari (1983), Neotectonic map of Italy, scale 1:500,000, 6 sheets, *Quad. Ric. Sci.*, *114/4*.

Andreotti, G. (1937), Il terremoto del 18 ottobre 1936, *Mem. Reale Istituto Veneto Sci. Lett. Arti*, *30*, 3–24.

Anonymous (2003), TRANSALP Conference, extended abstracts of oral and poster presentations, *Mem. Sci. Geol.*, *54*, 270.

Barbano, M. S., G. F. Gentile, and A. M. Riggio (1986), Il terremoto dell'Alpago-Cansiglio del 18.10.1936: Metodologia e problematiche legate allo studio di eventi recenti, in *Proceedings of the 5th National Conference G. N. G. T. S.*, pp. 47–60, Gruppo Natl. di Geofis. della Terra Solida, Rome.

Barnett, V., and T. Lewis (1978), *Outliers in Statistical Data*, 355 pp., John Wiley, Hoboken, N. J.

Beinat, A., F. Crosilla, R. Furlan-Radivo, C. Marchesini, G. Mozzi, G. Renner, G. Zambon, and A. Zanferrari (1988), Studio multidisciplinare dell'attività neotettonica nell'area di Caneva (Friuli), in *Proceedings of the 7th National Conference G. N. G. T. S.*, pp. 935–947, Gruppo Natl. di Geofis. della Terra Solida, Rome.

Benedetti, L., P. Tapponier, G. C. P. King, B. Meyer, and I. Manighetti (2000), Growth folding and active thrusting in the Montello region, Veneto, northern Italy, *J. Geophys. Res.*, *105*, 739–766.

Bertelli, L., L. Cantelli, A. Castellarin, R. Fantoni, A. Mosconi, M. Sella, and L. Selli (2003), Upper crustal style, shortening and deformation age in the Alps along the southern sector of the TRANSALP profile, *Mem. Sci. Geol.*, *54*, 123–126.

Bhattacharyya, J., A. F. Sheeland, K. Tiampo, and J. Rundle (1999), Using a genetic algorithm to model broadband regional waveforms for crustal structure in the western United States, *Bull. Seismol. Soc. Am.*, *89*, 202–214.

Boschi, E., G. Ferrari, P. Gasperini, E. Guidoboni, G. Smriglio, and G. Valensise (1995), *Catalogo dei Forti Terremoti in Italia dal 461 a.C. al 1980*, 973 pp., ING-SGA, Rome.

Boschi, E., et al. (1999), *Catalogo Parametrico dei Terremoti Italiani*, pp. 1–92, Gruppo di Lavoro ING, GNDT, SGIA, SSN, Editrice Compositori, Bologna, Italy.

Caputo, R., M. E. Poli, and A. Zanferrari (2003), Neogene-Quaternary twist tectonics in the eastern Southern Alps, Italy, *Mem. Sci. Geol.*, *54*, 155–158.

Carulli, G. B., R. Codermatz, F. Cucchi, L. Peruzza, F. Pettenati, A. Rebez, L. Sirovich, and D. Slejko (2002), A site-dependent seismic hazard map for the Friuli-Venezia Giulia region (NE Italy), in *Proceedings of the 12th European Conference on Earthquake Engineering* [CD-ROM], Elsevier Sci., New York.

Castaldini, D., and M. Panizza (1991), Inventario delle faglie attive tra i fiumi Po e Piave e il Lago di Como (Italia settentrionale), *Il Quat.*, *4*, 333–410.

Chiaruttini, C., and L. Siro (Sirovich) (1991), Focal mechanism of an earthquake of Baroque age in the 'Regno delle Due Sicilie' (southern Italy), *Tectonophysics*, *193*, 195–203.

Doglioni, C. (1990), Thrust tectonics examples from the Venetian Alps, *Stud. Geol. Camerti, Spec.*, 117–129.

Gasperini, P., F. Bernardini, G. Valensise, and E. Boschi (1999), Defining seismogenic sources from historical earthquake felt reports, *Bull. Seismol. Soc. Am.*, *89*, 34–110.

Gentile, F., F. Pettenati, and L. Sirovich (2004), Validation of the automatic nonlinear source inversion of the U.S. Geological Survey intensities of the Whittier Narrows, 1987 earthquake, *Bull. Seismol. Soc. Am.*, in press.

Goldberg, D. E. (1989), *Genetic Algorithms in Search, Optimization, and Machine Learning*, 460 pp., Addison-Wesley-Longman, Reading, Mass.

Hanks, T. C., and H. Kanamori (1979), A moment-magnitude scale, *J. Geophys. Res.*, *84*, 2348–2350.

Johnston, A. C. (1996), Seismic moment assessment of earthquakes in stable continental regions—I. Instrumental seismicity, *Geophys. J. Int.*, *124*, 381–414.

Kennett, B. L. N., and M. S. Sambridge (1992), Earthquake location—Genetic algorithms for teleseisms, *Phys. Earth Planet. Inter.*, *75*, 103–110.

Koper, K. D. L., M. E. Wysession, and D. A. Wiens (1999), Multimodal function optimization with a niching genetic algorithm, *Bull. Seismol. Soc. Am.*, *89*, 978–988.

Levine, D. (1996), User's guide to the PGAPack parallel genetic algorithm library, *Rep. ANL-95/18*, 73 pp., Argonne Natl. Lab., Argonne, Ill.

Madariaga, R., and P. Bernard (1985), Ray theoretical strong motion synthesis, *J. Geophys.*, *58*, 73–81.

Montone, P., A. Amato, A. Frepoli, M. T. Mariucci, and M. Cesaro (1996), Faulting regime and state of stress in Italy, in *Proceedings of the XXI General Assembly of the European Seismological Commission*, pp. 60–65, Eur. Seismol. Comm., Reykjavik, Iceland.

Moya, A., J. Aguirre, and K. Irikura (2000), Inversion of source parameters and site effects from strong ground motion records using genetic algorithms, *Bull. Seismol. Soc. Am.*, *90*, 977–992.

Ohta, Y., and K. Satoh (1980), Analyses on seismic intensity and earthquake disaster in the Caldiran earthquake, in *Engineering Seismological Studies on the 24 November 1976 Caldiran Earthquake in Turkey*, edited by Y. Ohta, pp. 89–117, Dept. Arch. Eng. Hokkaido Univ., Sapporo, Japan.

Okabe, A. B., B. Boots, K. Sugihara, and S. N. Chiu (2000), *Spatial Tessellation*, 2nd ed., 671 pp., John Wiley, Hoboken, N. J.

Panza, G. F., A. Craglietto, and P. Suhadolc (1991), Source geometry of historical events retrieved by synthetic isoseismals, *Tectonophysics*, *193*, 173–184.

Pellegrini, G. B., and A. Zanferrari (1980), Inquadramento strutturale ed evoluzione neotettonica dell'area compresa nei fogli 23 Belluno, 22 Feltre (p.p.), *Geodinamica*, *356*, 359–396.

Pettenati, F., and L. Sirovich (2003), Tests of source-parameter inversion of the U.S. Geological Survey intensities of the Whittier Narrows, 1987 earthquake, *Bull. Seismol. Soc. Am.*, *93*, 47–60.

Pettenati, F., L. Sirovich, and F. Cavallini (1999), Objective treatment, and synthesis of macroseismic intensity data sets using tessellation, *Bull. Seismol. Soc. Am.*, *89*, 1203–1213.

Pettenati, F., L. Sirovich, and F. Gentile (2003), Validation of some TRANSALP results (southern segment) by source inversion of the Cansiglio, 1936 earthquake, *Mem. Sci. Geol.*, *54*, 87–90.

Press, W. H., S. A. Teukolsky, W. T. Vetterling, and B. P. Flannery (1992), *Numerical Recipes in Fortran: The Art of Scientific Computing*, 2nd ed., 963 pp., Cambridge Univ. Press, New York.

Renner, G. (2000), Confronto fra epicentri macrosismici e strumentali dell'Italia nordorientale: Risultati preliminari, poster presented at the *80th National Meeting*, Ital. Geol. Soc., Trieste, Italy.

Sambridge, M., and K. Gallagher (1993), Earthquake hypocenter location using genetic algorithms, *Bull. Seismol. Soc. Am.*, *83*, 1467–1491.

Seeber, L., J. Armbruster, and S. Farhatullah (1980), Seismic activity at the Tarbela dam site and surrounding area, *Geol. Bull. Univ. Peshawar*, *13*, 169–191.

Sieberg, A. (1930), Geologie der Erdbeben, *Handboch Geophys.*, *2*(4), 550–555.

Siro (Sirovich), L. (1982), Emergency microzonations by Italian Geodynamics Project after November 23, 1980 earthquake: A short technical report, paper presented at the 3rd International Conference on Microzonation, Seattle, Wash., 28 June–1 July.

Siro (Sirovich), L., and D. Slejko (1982), Space-time evolution of the 1977–1980 seismicity in the Friuli area and its seismotectonic implications, *Boll. Geof. Teor. Appl.*, *24*, 67–77.

Sirovich, L. (1996a), A simple algorithm for tracing out synthetic isoseismals, *Bull. Seismol. Soc. Am.*, *86*, 1019–1027.

Sirovich, L. (1996b), Synthetic isoseismals of two Californian earthquakes, *Nat. Haz.*, *14*, 23–37.

Sirovich, L. (1997), Synthetic isoseismals of three earthquakes in California-Nevada, *Soil Dyn. Earthquake Eng.*, *16*, 353–362.

Sirovich, L., and F. Pettenati (2001), Test of source parameters inversion of the intensities of a 54,000-death shock of the XVII century in SE Sicily, *Bull. Seismol. Soc. Am.*, *91*, 792–811.

Sirovich, L., F. Pettenati, and C. Chiaruttini (2001), Test of source-parameter inversion of intensity data, *Nat. Haz.*, *24*, 105–131.

Slejko, D., et al. (1987), Modello sismotettonico dell'Italia nord-Orientale, *Rep. CNR-GNDT N°1*, 82 pp., Litografia Ricci, Trieste, Italy.

Slejko, D., et al. (1989), Seismotectonics of the eastern Southern-Alps: A review, *Boll. Geof. Teor. Appl.*, *31*, 109–136.

Soramel, E., and G. Zaia (1985), Rilevamento geologico del settore meridionale del Cansiglio, graduate thesis, 61 pp., Padua Univ., Italy.

Sponheuer, W. (1960), Berechnungsverfahren mit schrittweiser Noeherung, in Methoden zur Herdtiefen Bestimmung in der Makroseismik, in *Freiberger Forschungshefte C88*, edited by W. Sponheuer, pp. 16–32, Akademie Verlag, Berlin.

Spudich, P., and L. N. Frazer (1984), Use of ray theory to calculate high-frequency radiation from earthquake sources having spatially variable rupture velocity and stress drop, *Bull. Seismol. Soc. Am.*, *74*, 2061–2082.

TRANSALP Working Group (2001), European orogenic processes research transects the eastern Alps, *Eos Trans. AGU*, *82*(40), 453–461.

Valensise, G., and D. Pantosti (Eds.) (2001), Database of potential sources for earthquakes larger than M 5.5 in Italy, *Ann. Geofis.*, *44*(4), suppl., 180 pp.

Wells, D. L., and K. J. Coppersmith (1994), New empirical relationships among magnitude, rupture length, rupture width, rupture area, and surface displacement, *Bull. Seismol. Soc. Am.*, *84*, 974–1002.

Zanferrari, A., et al. (1982), Evoluzione neotettonica dell'Italia nord-orientale, *Mem. Sci. Geol.*, *35*, 355–376.

Zeng, Y., K. Aki, and T.-L. Teng (1993), Source inversion of the 1987 Whittier Narrows earthquake, California, using the isochrone method, *Bull. Seismol. Soc. Am.*, *83*, 358–377.

Zhou, R., R. Tajima, and P. L. Stoffa (1995), Application of genetic algorithms to constrain near-source velocity structure for the 1989 Sichuan earthquakes, *Bull. Seismol. Soc. Am.*, *85*, 590–605.

F. Pettenati and L. Sirovich, Istituto Nazionale di Oceanografia e di Geofisica Sperimentale, Borgo Grotta Gigante 42C, I-34010 Sgonico Trieste, Italy. (fpettenati@ogs.trieste.it; sirovich@ogs.trieste.it)